Journal of Power Sources 196 (2011) 2269–2273

Contents lists available at ScienceDirect

Journal of Power Sources

journal homepage: www.elsevier.com/locate/jpowsour

Short communication

Microstructural controls of titanate nanosheet composites using carbon fibers and high-rate electrode properties for lithium ion secondary batteries

Shinya Suzuki*, Masaru Miyayama

Research Center for Advanced Science and Technology, The University of Tokyo, 4-6-1 Komaba, Meguro-ku, Tokyo 153-8904, Japan

ARTICLE INFO

Article history:
Received 23 July 2010
Received in revised form
17 September 2010
Accepted 21 September 2010
Available online 29 September 2010

Keywords:
Nanosheets
Titanate
Carbon fibers
Porous electrode
High-rate capability
Lithium ion secondary batteries

ABSTRACT

Composite electrodes of reassembled titanate and two kinds of carbon fibers were prepared and their high-rate electrode properties were examined. Multi-walled carbon nanotubes (MWNT) and vapor-grown carbon fibers (VGCF) were used for preparing the composites. The electronic conductivity of the MWNT composites increased with increasing contents of MWNT and exhibited a typical insulator-conductor transition. The MWNT composite with a MWNT content of 50 wt.% showed a capacity of 150 ± 5 mAh (g titanate)$^{-1}$ at a discharge rate of 0.67 C, and did not show a good high-rate capability due to the large content of hydrated water. The effect of the porous structure of the electrodes was revealed in the high-rate electrode properties of the microstructurally controlled composites with both MWNT and VGCF. The composites with 50 wt.% VGCF and 10 wt.% MWNT showed a reversible capacity of approximately 160 mAh (g titanate)$^{-1}$ at a discharge rate of 0.63 C and almost no capacity fading at relatively large discharge rate up to 19 C. A composite electrode with excellent high-rate capability was obtained by the microstructural control with carbon fibers.

1. Introduction

There is a strong industrial demand for high power-capable power sources for electric/hybrid vehicles. Today most portable electronic devices are powered by lithium ion secondary batteries (LIBs) with high energy density and good cycleability. LIBs are also attractive energy storage devices for high power applications [1]. However, there are hurdles for most of electrode materials of LIBs in high power uses. The diffusion of lithium ion in the solid phase is rather slow (e.g., the diffusion coefficients of lithium ion in most intercalation host materials are in the range of 10^{-9} to 10^{-13} cm^2 s^{-1}), and the electronic conductivity of lithium intercalation host materials is usually too low to sustain a large current.

In most cases for lithium ion secondary batteries, the lithium intercalation capacities at a relatively large current density operation are limited by the slow diffusion of lithium ion in the solid phase. Decreasing the particle size of the cathode material is a common way to reduce the capacity fading during large current operation [2,3]. However, decreasing the particle size of the cathode material leads to another problem concerning the cycling durability. It is well known that the contact resistance between the cathode materials and the carbon powder as conducting additives must remain as small as possible in order to obtain good cycling durability. As the particle size becomes smaller and equivalent to that of the carbon powder, the mixture of the two becomes less homogeneous and it is difficult to obtain good electronic contact. Chen et al. reported that the contact resistance of the cathode with $LiCoO_2$ at a size below 100 nm was much larger than that with commercial $LiCoO_2$ [4]. As a result, as the particle size becomes smaller, the rate of capacity fade during the cycling operation becomes faster. The homogeneous mixing of nanometer-size cathode materials and carbon powder is a significant problem for large current density operation, in other words, high-rate operation.

To preserve the benefits of electrochemistry of nanoscale materials, and to achieve high-rate capabilities, various microstructural controls have been reported. A recent example is the Fe_3O_4 nanoparticles deposited on Cu nanorods grown onto the current collector reported by Taberna et al. [5]. The electrons are supplied from Cu nanorods to all Fe_3O_4 nanoparticles. The openness of the basic nanostructure of Cu nanorods facilitates the access of ion-conducting liquid electrolyte to the whole surface of Fe_3O_4 nanoparticles. A perfect supply of electrons and ions to the nanoparticles enables the extremely high rate of the reactions.

Recently, nanosheets have been synthesized as a new class of nanoscale materials by disintegrating a layered compound into a single layer or several layers [6,7]. These unilamellar or multilamellar crystallites have a thickness on the order of nanometers, with lateral dimensions of submicro- to micrometers. Nanosheets

* Corresponding author at: Miyayama Lab., Research Center for Advanced Science and Technology, The University of Tokyo, 4-6-1 Komaba, Meguro-ku, Tokyo 153-8904, Japan. Tel.: +81 3 5452 5082; fax: +81 3 5452 5083.
E-mail address: sin@crm.rcast.u-tokyo.ac.jp (S. Suzuki).

0378-7753/$ – see front matter © 2010 Elsevier B.V. All rights reserved.
doi:10.1016/j.jpowsour.2010.09.062

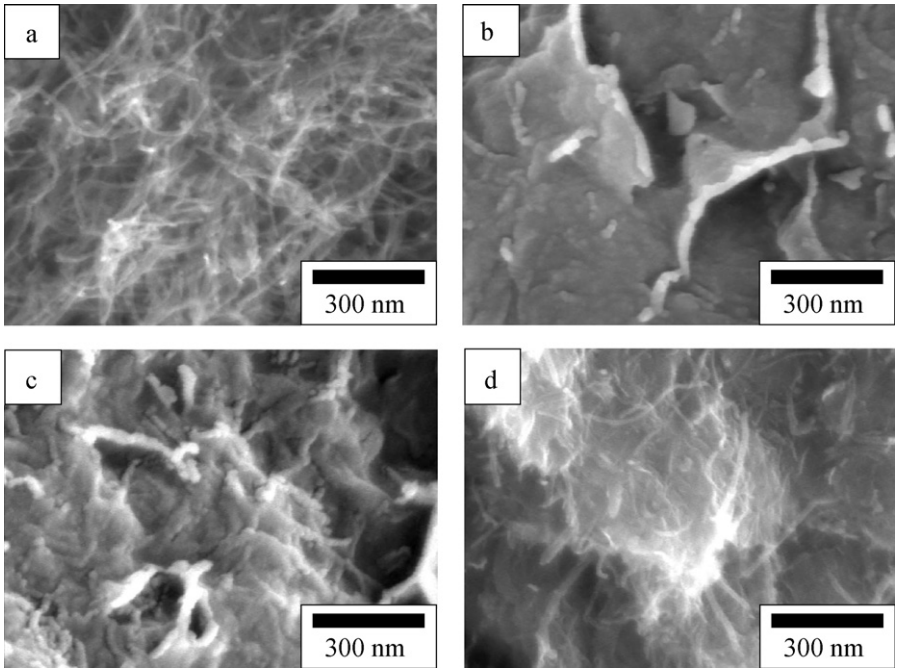

Fig. 1. SEM images for (a) cut MWNT, (b) RTiNS/MWNT(5), (c) RTiNS/MWNT(20), and (d) RTiNS/MWNT(50).

are thus crystallites with an attractive potential for use as a component of microstructurally controlled lithium intercalation host materials, since nanosheets are obtained as a colloidal suspension to which a variety of sol–gel processing methods can be applied [8,9].

We previously reported the synthesis and high-rate electrode properties of a titanate nanosheet composite with vapor-grown carbon fibers [10]. The composite with vapor-grown carbon fibers exhibited a relatively large capacity of 135 mAh g^{-1} at a large discharge rate of 53 C, which corresponds to about 70% of the discharge capacity at a relatively small current discharge rate of 0.53 C. The composites with carbon fibers exhibited a good performance as high-rate lithium insertion electrodes. Increased high-rate capability is expected by further microstructural controls.

In the present study, microstructural control of the electrodes using nanosheets as building blocks was attempted by mixing titanate nanosheets, carbon nanotubes, and vapor-grown carbon fibers. The effect of the microstructure on the high-rate capability was investigated.

2. Experimental

A fibrous tetratitanate $H_2Ti_4O_9{\cdot}1.9H_2O$ (Otsuka Chemical Co., Tokushima, Japan) was used as the starting material. A weighed amount (1.0 g) of a fibrous tetratitanate powder was stirred in 200 cm^3 of aqueous solution of tetrabutylammonium hydroxide for 10 days at room temperature, resulting in the exfoliation of tetratitanate [11]. A twofold molar amount of tetrabutylammonium hydroxide to tetratitanate was used in the reaction. Relatively large particles were centrifugally separated at 2000 rpm. The supernatant was used for preparing the composites.

The bundles of multi-walled carbon nanotubes (Aldrich, Milwaukee, WI), denoted as MWNT hereafter, were separated and the individual MWNT was cut using the process reported by Liu et al. [12]. In brief, the raw MWNT were suspended in a 3:1 mixture of concentrated H_2SO_4/HNO_3 and sonicated in a water bath for 24 h, then stirred in a 4:1 mixture of concentrated H_2SO_4 and 30% aqueous solution of H_2O_2 for 30 min. VGCF (Showa Denko, Tokyo, Japan) with 10 μm length and 150 nm diameter was used as received.

The cut MWNT and VGCF were dispersed in a colloidal suspension of tetratitanate nanosheets with various weight ratios with no surfactant. The obtained dispersions were reacted with 0.1 mol dm^{-3} HCl for the reassembly of nanosheets, and the precipitates were collected on a filter with pores of 100 nm in size, washed with distilled water, and dried at ambient temperature. The precipitates were heated at 200 °C for 2 h to convert the tetratitanate into octatitanate [10,13,14].

The morphologies and the textures of the obtained composites were observed by scanning electron microscopy (SEM) on an S-4500 (Hitachi, Tokyo, Japan). The microstructure of the composite was characterized by mercury porosimetry on a Pore Sizer 9320 (Micromeritics, Norcross, GA) and by N_2 adsorption measurement on a Tristar 3000 (Micromeritics). The weight ratio of the titanate in the composites and the amount of hydrated water in the titanate were determined by thermal gravimetry (TG) on a TG8120 (Rigaku, Tokyo, Japan) and inductively coupled plasma (ICP) spectroscopy using an SPS4000 (Seiko Instruments, Tokyo, Japan).

The samples for electric and electrochemical measurements were fabricated by pressing a mixture of 90 wt.% obtained composites and 10 wt.% binder (PTFE; DuPont) at 100 MPa. The disk-shaped samples of 10 mm in diameter and approximately 1 mm in thickness were prepared for the tests of electronic conductivity. The electronic conductivity was measured by DC using the two-point probe method.

The electrodes for electrochemical measurements of approximately 0.15 mm thickness were prepared by pressing the mixture with 10 wt.% PTFE binder onto Ni mesh. The tap-density for the electrodes was approximately 1.3 g cm^{-3}. The mass of the composite was 20 mg cm^{-2}. Electrochemical measurements were performed using a three-electrode cell with lithium strips as the reference and counter electrodes, and the prepared electrode as a working electrode. The electrolyte solution was 1 mol dm^{-3} lithium perchlorate in propylene carbonate (Kishida Chemical Co., Osaka, Japan). Galvanostatic discharge/charge tests were carried out in the voltage range from 1.2 V to 3.6 V (vs. Li/Li^+) on a HAG-5001 potentiostat/galvanostat (Hokuto Denko, Tokyo, Japan).

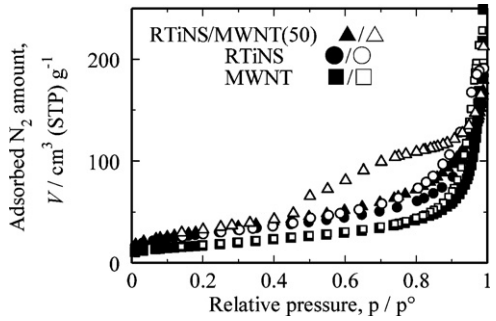

Fig. 2. Nitrogen adsorption/desorption isotherms for RTiNS/MWNT(50), RTiNS, and MWNT. The closed and open marks indicate adsorption and desorption isotherms, respectively.

3. Results and discussion

The size of tetratitanate nanosheets used for the preparation of the composite was as follows: length ~1 μm, width 100–300 nm, thickness 1.8 nm [10]. The composites with MWNT and VGCF were denoted as RTiNS/MWNT(x) and RTiNS/VGCF(x) with the content of carbon fibers x/wt.% in parenthesis. A powder prepared by a reassembly of tetratitanate nanosheets and subsequent heat treatment was denoted as RTiNS.

3.1. Electronic conductivity of the composites with MWNT

Fig. 1(a) shows a SEM image for the cut MWNT. MWNT of 20 nm in diameter was observed. Fig. 1(b)–(d) shows SEM images for the composites with various contents of MWNT. MWNT was clearly observed only in RTiNS/MWNT(50) among the composites. Other composites had a rough texture. The rough texture of the composites seemed to have been caused by the existence of MWNT.

Fig. 2 shows nitrogen adsorption/desorption isotherms for RTiNS/MWNT(50), RTiNS, and MWNT. An isotherm of RTiNS/MWNT(50) exhibited a strong hysteresis loop in the p/p° region from 0.45 to 0.95, and isotherms of RTiNS and MWNT did not show such a strong hysteresis loop. This hysteresis indicates the formation of pore of 3–8 nm in diameter in RTiNS/MWNT(50) by mixing of nanosheets and MWNT. BET surface areas of RTiNS/MWNT(50), RTiNS, and MWNT were 110, 100, and 60 m^2 g^{-1}, respectively. RTiNS/MWNT(50) showed a larger surface area than RTiNS and MWNT. The SEM observation and N_2 adsorption measurement indicate that MWNT locally prevents nanosheets from stacking. The pore in RTiNS/MWNT(50) is probably formed beside MWNT which was interposed between nanosheets. These results suggest that fine and homogeneous composites were obtained by a reassembly of the homogeneous mixture of dispersed MWNT in a colloidal suspension of nanosheets. It is reported that interaction between MWNT and TiO_2 was promoted by surface oxidation of MWNT [15]. This interaction is expected between titanate nanosheets and cut MWNT because MWNT was cut by the reaction with oxidative mixed acid, and would contribute to form homogeneous composite.

Fig. 3 shows the electronic conductivity of RTiNS/MWNT(x) with various contents of MWNT. The electronic conductivity of the composites increased with increasing contents of MWNT and exhibited a typical insulator–conductor transition. The percolation threshold existed between 2 and 5 wt.%. This small value of the percolation threshold was attributed to the enormous aspect ratio of MWNT [16]. The percolation threshold was reported between 1 and 2 wt.% for the composite of TiO_2 nanoparticles and MWNT [15]. The observed value was slightly larger than the reported value. This would be due to the microstructure of RTiNS/MWNT(x) shown in Fig. 1 where MWNT was interposed between nanosheets. The electronic conductivity for RTiNS/MWNT(50) was 8.5×10^{-2} S cm^{-1}, and was sufficient to sustain a large current under high-rate operation.

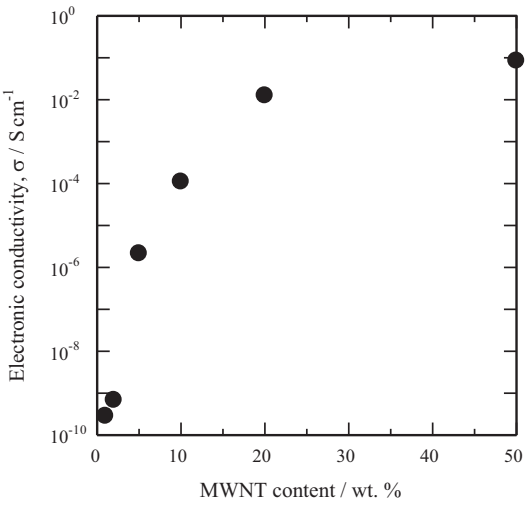

Fig. 3. Electronic conductivities of RTiNS/MWNT(x) as a function of the content of MWNT, x.

3.2. High-rate electrode properties of the composites with 50 wt.% carbon fibers

We demonstrated in the former section that a homogeneous composite of nanosheets and MWNT can be obtained, and RTiNS/MWNT(50) showed sufficiently high electronic conductivity to sustain large current density under high-rate operation. Good high-rate capability is expected for RTiNS/MWNT(50). In addition, we previously reported an excellent high-rate capability of titanate nanosheets composites with VGCF [10]. RTiNS/VGCF(50) was an inhomogeneous mixture, that is, a mixture of VGCF and lumps of reassembled titanate with a size of 2–3 μm. Increased high-rate capability is expected by addition of electronic conductivity to these lumps of reassembled titanate by homogeneous mixing of MWNT. In this section, two MWNT composites RTiNS/MWNT50) and RTiNS/VGCF(40) + MWNT(10) were prepared and their high-rate electrode properties were examined.

Fig. 4 shows an SEM image of RTiNS/VGCF(40) + MWNT(10). VGCF and lumps of reassembled titanate with a size of 2–3 μm were observed. MWNT were not clearly observed, indicating that the homogenous composite of reassembled titanate and MWNT was obtained as described in the former sec-

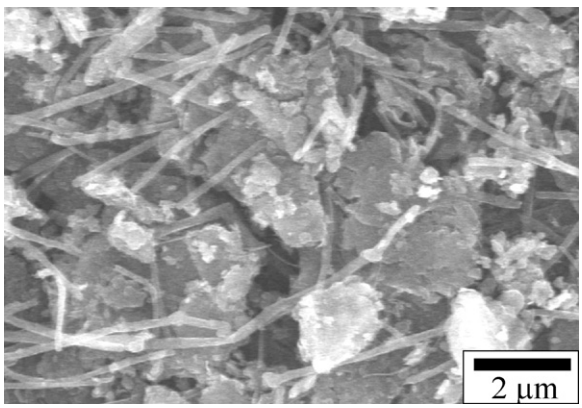

Fig. 4. SEM image for RTiNS/VGCF(40) + MWNT(10).

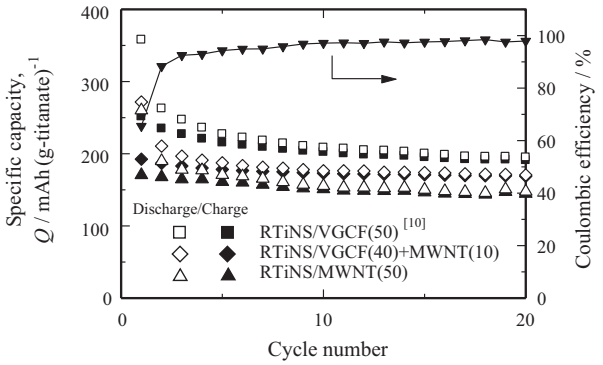

Fig. 5. Cycling performance for RTiNS/MWNT(50) and RTiNS/VGCF(40) + MWNT(10) at constant discharge/charge rates of 0.67 C and 0.61 C, respectively (100 mA g^{-1}). The coulombic efficiency for RTiNS/MWNT(50) is also shown.

tion. Consequently, RTiNS/VGCF(40) + MWNT(10) had the expected microstructure.

Fig. 5 shows the cycling performance for RTiNS/MWNT(50) and RTiNS/VGCF(40) + MWNT(10) in comparison with that of RTiNS/VGCF(50). The discharge and charge capacities are normalized by the weight of reassembled titanate. RTiNS/MWNT(50) and RTiNS/VGCF(40) + MWNT(10) exhibited relatively large irreversible capacities in the first several cycles. This irreversible capacity is a feature of reassembled titanate, as we previously reported [14,17]. The irreversible capacity decreased with the discharge/charge cycles, and RTiNS/MWNT(50) and RTiNS/VGCF(40) + MWNT(10) exhibited a reversible capacity of 150 ± 5 and 165 ± 5 mAh g^{-1}, respectively, and a coulombic efficiency up to 97% at the 10th cycle. The capacity values indicated hereafter are those obtained after the 10th cycle. The capacities (sum of double layer capacitance and faradaic pseudocapacitance) of VGCF and MWNT were 3 and 15 mAh g^{-1}, respectively. Consequently, the capacity of RTiNS/MWNT(50) includes the capacity of up to 15 mAh g^{-1} which is caused by MWNT. The composite with MWNT showed smaller capacity than the reassembled titanate (170 mAh g^{-1}) [9] or the composite with VGCF (190 mAh g^{-1}) [10]. The reassembled titanates have hydrated water molecules between the oxide layers. The chemical formula of reassembled titanates in the composite was determined by thermogravimetry, and those of reassembled octatitanate, RTiNS/VGCF(50), RTiNS/VGCF(40) + MWNT(10) and RTiNS/MWNT(50) were $H_2Ti_8O_{17}{\cdot}0.43H_2O$, $H_2Ti_8O_{17}{\cdot}1.1H_2O$, $H_2Ti_8O_{17}{\cdot}2.0H_2O$ and $H_2Ti_8O_{17}{\cdot}3.6H_2O$ (or $H_2Ti_4O_9{\cdot}1.3H_2O$), respectively. A relatively large amount of hydrated water in MWNT composites is responsible for the small capacity, since the capacity is normalized by the weight of titanate including hydrated water. The transformation reaction from layer-structured tetratitanate to tunnel-structured octatitanate is accompanied by dehydration of water molecules between the oxide layers. MWNT interposed between nanosheets locally prevents oxide layers from stacking and transforming of tetratitanate into octatitanate.

Fig. 6(a) shows the discharge curves for RTiNS/MWNT(50) measured at various current densities. The discharge capacity gradually decreased with increasing current density. RTiNS/MWNT(50) exhibited a discharge capacity of 80 mAh g^{-1} at a discharge rate of 3.3 C. RTiNS/MWNT(50) did not show a good high-rate capability. In our previous study, an octatitanate with a small amount of hydrated water exhibited a larger capacity than that with a relatively large amount of hydrated water at a large current operation [18]. The capacity fading for RTiNS/MWNT(50) at a large current operation is due to the relatively large amount of hydrated water contained in the reassembled titanate.

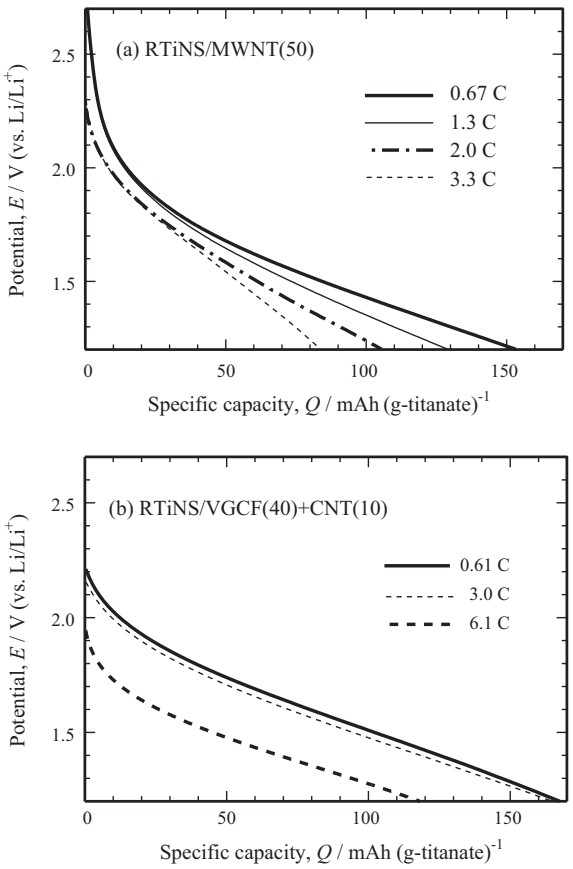

Fig. 6. Discharge curves for (a) RTiNS/MWNT(50) and (b) RTiNS/VGCF(40) + MWNT(10) measured at various current densities.

Fig. 6(b) shows the discharge curves for RTiNS/VGCF(40) + MWNT(10) measured at various current densities. Almost constant discharge capacities of approximately 165 mAh g^{-1} were observed at a discharge rate less than 6.1 C, and a capacity of 115 mAh g^{-1} was exhibited at a relatively large discharge rate of 6.1 C. We reported previously that RTiNS/VGCF(50) showed a large capacity of 165 mAh g^{-1} at a discharge rate of 5.3 C [5]. RTiNS/VGCF(40) + MWNT(10) showed a better rate capability than RTiNS/MWNT(50), but an inferior rate capability compared to RTiNS/VGCF(50). The inferior rate capability was clearly due to the potential drop, and potential drop is usually caused by an insufficient electronic conductivity. The electronic conductivity of RTiNS/VGCF(40) + MWNT(10) was 9.6×10^{-2} S cm^{-1}, as measured by DC. The ohmic drop at a discharge rate of 6.1 C based on the electronic conductivity was estimated to be 3 mV. Consequently, the potential drop was not mainly caused by electronic conductivity. To clarify the reason for the potential drop, the pore size distribution for RTiNS/VGCF(40) + MWNT(10) was measured, and the results are shown in Fig. 7 in comparison with those for RTiNS/VGCF(50). The pore size distribution for RTiNS/VGCF(40) + MWNT(10) showed a maximum value around a pore diameter of 150 nm, and it was smaller than that of RTiNS/VGCF(50). In the composite with VGCF, the lamps of reassembled titanate partially occupied the space among VGCF. RTiNS/VGCF(40) + MWNT(10) showed a smaller pore size and pore volume than RTiNS/VGCF(50) due to the relatively small content of the VGCF generating the pores. When these composites are used as electrodes, electrolyte solution penetrates into the pores through the electrodes. The pores work as fast lithium ion transportation paths with the help of electrolyte solution [5,19,20]. The inferior high-rate capability of RTiNS/VGCF(40) + MWNT(10) compared to RTiNS/VGCF(50) would have been caused by insuffi-

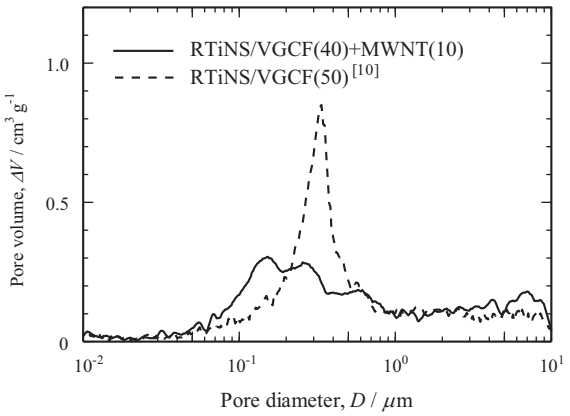

Fig. 7. Pore size distribution for RTiNS/VGCF(40) + MWNT(10) in comparison with that of RTiNS/VGCF(50).

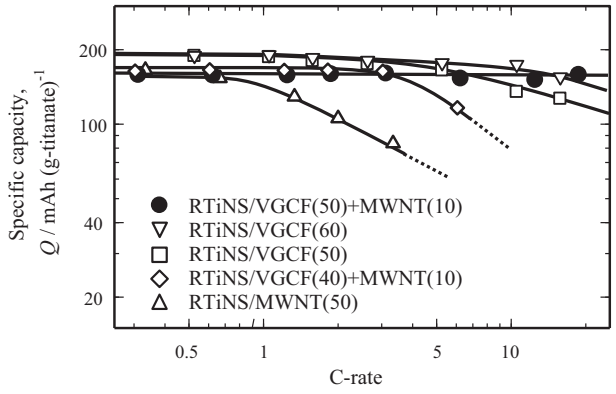

Fig. 8. Specific capacities of the nanosheet composites with various carbon fiber contents as a function of discharge rate.

cient lithium transportation through the electrode due to the small pore size and pore volume in the composite.

3.3. High-rate composite electrode with two kinds of carbon fibers

Increased high-rate capability is expected by simultaneous achievement of both of the following: (i) addition of electronic conductivity to these lumps of reassembled titanate by homogeneous mixing of MWNT; and (ii) retention of a porous structure with relatively large pore size and pore volume by the mixing with VGCF. Therefore, we prepared RTiNS/VGCF(50) + MWNT(10) and examined its high-rate electrode property. We also prepared RTiNS/VGCF(60) and its high-rate electrode property were compared with RTiNS/VGCF(50) + MWNT(10). RTiNS/VGCF(50) + MWNT(10) showed a reversible capacity of approximately 160 mAh g^{-1} at a discharge rate of 0.63 C at the 10th cycle. Discharge/charge tests were conducted at various current densities, and the relationship between the capacity and current density is shown in Fig. 8. Fig. 8 also shows the relationship for RTiNS/VGCF(60), RTiNS/MWNT(50), RTiNS/VGCF(40) + MWNT(10) and RTiNS/VGCF(50). RTiNS/VGCF(50) + MWNT(10) showed almost no capacity fading at a relatively large discharge rate up to 19 C. RTiNS/VGCF(50) + MWNT(10) showed excellent high-rate capability. Hierarchical electronic conduction by both VGCF and MWNT [21], and a porous structure with large pore size and large pore volume contributed to the excellent high-rate capability. In this study, therefore, we demonstrated that flexibility of microstructural controls using nanosheets, and composite electrodes with excellent high-rate capability can be obtained by the microstructural control with carbon fibers.

4. Conclusions

The homogeneous composites were obtained by a reassembly of the dispersion of MWNT in a colloidal suspension of nanosheets. The electronic conductivity of the composites increased with increasing contents of MWNT and exhibited a typical insulator–conductor transition. The percolation threshold existed between 2 and 5 wt.%. The MWNT composite with a MWNT content of 50 wt.% showed a capacity of 150 ± 5 mAh g^{-1} at a discharge rate of 0.67 C, and did not show a good high-rate capability due to the large content of hydrated water. The composites with 50 wt.% VGCF and 10 wt.% MWNT showed a reversible capacity of approximately 160 mAh g^{-1} at a discharge rate of 0.63 C and almost no capacity fading at relatively large discharge rate up to 19 C. The porous structure of the composites contributed to the excellent high-rate capability, since the pores work as fast lithium ion transportation paths with the help of the electrolyte solution penetrated into the pores. A composite electrode with excellent high-rate capability was obtained by the microstructural control with carbon fibers.

References

[1] D. Linden, T.B. Reddy, Handbook of Batteries, McGraw-Hill, New York, 2001.
[2] H. Chen, C.P. Grey, Adv. Mater. 20 (2008) 2206–2210.
[3] E. Hosono, T. Kudo, I. Honma, H. Matsuda, H. Zhou, Nano Lett. 9 (2009) 1045–1051.
[4] H. Chen, X. Qiu, W. Zhu, P. Hagenmuller, Electrochem. Commun. 4 (2002) 488–491.
[5] P.L. Taberna, S. Mitra, P. Poizot, P. Simon, J.-M. Tarascon, Nat. Mater. 5 (2006) 567–573.
[6] T. Sasaki, M. Watanabe, H. Hashizume, H. Yamada, H. Nakazawa, J. Am. Chem. Soc. 118 (1996) 8329–8335.
[7] T. Sasaki, M. Watanabe, J. Am. Chem. Soc. 120 (1998) 4682–4689.
[8] L. Wang, T. Sasaki, Y. Ebina, K. Kurashima, M. Watanabe, Chem. Mater. 14 (2002) 4827–4832.
[9] M. Muramatsu, K. Akatsuka, Y. Ebina, K. Wang, T. Sasaki, T. Ishida, K. Miyake, M. Haga, Langmuir 21 (2005) 6590–6595.
[10] S. Suzuki, M. Miyayama, J. Electrochem. Soc. 154 (2007) A438–A443.
[11] W. Sugimoto, O. Terabayashi, Y. Murakami, Y. Takasu, J. Mater. Chem. 12 (2002) 3814–3818.
[12] J. Liu, A.G. Rinzler, H. Dai, J.H. Hafner, R.K. Bradley, P.J. Boul, A. Lu, T. Iverson, K. Shelimov, C.B. Huffman, F. Rodriguez-Macias, Y.-S. Shon, T.R. Lee, D.T. Colbert, R.E. Smalley, Science 280 (1998) 1253–1256.
[13] H. Izawa, S. Kikkawa, M. Koizumi, J. Phys. Chem. 86 (1982) 5023–5026.
[14] S. Suzuki, M. Miyayama, J. Phys. Chem. B 110 (2006) 4731–4734.
[15] L. Kavan, R. Bacsa, M. Tunckol, P. Serp, S.M. Zakeeruddin, F. Le Formal, M. Zukalova, M. Graetzel, J. Power Sources 195 (2010) 5360–5369.
[16] K. Ahmad, W. Pan, S.-L. Shi, Appl. Phys. Lett. 89 (2006) 133122.
[17] S. Suzuki, M. Miyayama, Key Eng. Mater. 248 (2003) 151–154.
[18] S. Suzuki, M. Miyayama, J. Ceram. Soc. Jpn, in press.
[19] H. Zhou, D. Li, M. Hibino, I. Honma, Angew. Chem. Int. 44 (2005) 797–802.
[20] R. Dominko, M. Bele, J.-M. Goupil, M. Gaberscek, D. Hanzel, I. Arcon, J. Jamnik, Chem. Mater. 19 (2007) 2960–2969.
[21] I. Moriguchi, R. Hidaka, H. Yamada, T. Kudo, H. Murakami, N. Nakashima, Adv. Mater. 18 (2006) 69–73.